IOP Publishing European Journal of Physics

Eur. J. Phys. **28** (2007) 1105–1124 doi:10.1088/0143-0807/28/6/008

Radiation trapping in 1D using the Markov chain formalism: a computational physics project

A R Alves-Pereira[1], E J Nunes-Pereira[1], J M G Martinho[2] and M N Berberan-Santos[2]

[1] Universidade do Minho, Escola de Ciências, Centro de Física, 4710-057 Braga, Portugal
[2] Centro de Química-Física Molecular, Instituto Superior Técnico, 1049-001 Lisboa, Portugal

E-mail: epereira@fisica.uminho.pt

Received 8 May 2007, in final form 31 July 2007
Published 12 September 2007
Online at stacks.iop.org/EJP/28/1105

Abstract

A computational model study for atomic radiation trapping is presented with an audience non-specialized in radiation transport in mind. The level of presentation is adequate for a final undergraduate or beginning graduate project in a computational physics instruction. The dynamics of resonance radiation transport is discussed using a theoretical model known as the multiple scattering representation. This model is compared with the alternative Holstein's ansatz, reinterpreting the fundamental mode as the one associated with a relaxed stationary spatial distribution of excitation. Its computational implementation is done making use of the stochastic Markov chain formalism. A comprehensive discussion of its rationale as well as fine implementation details are presented. The simplest case of complete frequency redistribution in a two-level system is considered for a unidimensional geometry. Nevertheless, the model study discusses at length the influence of the spectral distributions, overall opacity and emission quantum yield for trapping distorted ensemble quantities stressing physical insight and using only straightforward algorithmic concepts. Overall relaxation parameters (ensemble emission yield and lifetime) as well as steady-state quantities (spectra and spatial distribution) are calculated as a function of intrinsic emission yield, opacity and external excitation mode for Doppler, Lorentz and Voigt lineshapes, respectively, with the fundamental mode contribution singled out.

1. Introduction

In optically thick media, electronic excitation energy can undergo several reabsorption and reemission events before either escaping to the surroundings or being converted into thermal

energy by means of collisional deactivation. Atomic *radiation trapping* is also known as *imprisonment of resonance radiation*, *reabsorption*, *self-absorption*, *line transfer*, *radiation diffusion* or *multiple scattering* of resonance radiation. This *resonance radiation trapping* is important in areas as diverse as stellar atmospheres [1], plasmas and atomic vapour luminescence [2], terrestrial atmosphere and ocean optics [3], molecular luminescence [4], infrared radiative transfer [5] and cold atoms [6]. From the point of view of economically important applications, electric discharge lamps are still the most important application [7] even though electrodeless fluorescence lamps [8] and large area plasma display panels [9] are gaining an increasing importance.

In spite of its importance from the fundamental physics point of view as well as from the need to control trapping in practical applications, the discussion of the physical implications of radiation trapping at the level of the nonspecialist has been hampered by several factors, most notably, the intricate computational technicalities that were developed over the decades to obtain useful estimates of trapping-dependent quantities in practical situations. In this context, the present contribution should appeal to a broad audience and be valuable in the context of a final undergraduate and beginning graduate physics instruction since, although it uses only straightforward computational resources and concepts, it nevertheless allows at least a semi-quantitative detailed discussion of the physical implications of a wide range of factors affecting trapping efficiency and dynamics.

Section 2 discusses the way the dynamics of incoherent trapping is usually taken into account. The two standard alternative approaches to quantify trapping, the so-called Holstein mode expansion and the multiple scattering representation (MSR), are outlined giving particular emphasis on the connection between both through the (re)interpretation of the Holstein fundamental mode as the one associated with a relaxed nonchanging spatial distribution of excitation. Expressions for the macroscopic relaxation parameters (emission yield and lifetime) and steady-state quantities are derived within the MSR framework but with the fundamental mode contribution singled-out. The estimation of these quantities is then implemented using a simple Markov chain algorithm to quantify incoherent trapping in a computational model study for two-level atomic models. This is done in section 3 in which the rationale as well as critical implementation details are given. Section 4 presents the results and their discussion at length. Particular emphasis is placed on the discussion of the physical implications of the range of factors affecting trapping including the spectral lineshape, and the conditions of creation of initial excitation (collisional or photoexcitation). A thorough discussion of the conditions for which the use of Holstein's fundamental mode alone is a tolerable approximation is included. Finally, the main conclusions are summarized in section 5.

2. Dynamics of incoherent trapping

2.1. Characteristic scales

Radiation trapping studies should be cast in dimensionless coordinates since this increases computational efficiency and, more importantly, defines characteristic scales or universal conditions. The quantities most directly amenable to define characteristic scales in trapping are time, distance and optical frequency. The scaled time is $t = \Gamma t'$, where Γ is the global deactivation rate constant. The dimensionless distance is sometimes called the *opacity* or *optical density*. $k(x) = k_0\Phi(x)/\Phi(0)$ is the single line monochromatic opacity (k_0 is the corresponding centre-of-line value which, for homogeneously distributed species along a given pathlength l, is $k_0 = n\sigma_0 l$, with n and σ_0 being the numerical density and the

centre-of-line absorption cross section, respectively) and the absorption lineshape is given by the normalized spectral distribution $\Phi(x)$ (so that $\int_{-\infty}^{+\infty}\Phi(x)\,\mathrm{d}x = 1$). x is used to represent the optical frequency (see below). Finally, the overall (reflecting the whole of the spectral distribution) dimensionless opacity is $r = \int_{-\infty}^{+\infty}k(x)\,\mathrm{d}x = \frac{k_0}{\Phi(0)}$ and this defines the characteristic lengthscale for trapping.

For two-level atomic models, the intrinsic (i.e. undistorted by trapping) spectrum is usually described by a Doppler, $\Phi_D(x) = \frac{1}{\sqrt{\pi}}\,\mathrm{e}^{-x^2}$, a Lorentz, $\Phi_L(x) = \frac{1}{\pi}\frac{1}{1+x^2}$, or a Voigt, $\Phi_V(x) = \frac{a}{\pi^{3/2}}\int_{-\infty}^{+\infty}\frac{\mathrm{e}^{-u^2}}{a^2+(x-u)^2}\,\mathrm{d}u$, spectral distribution. The Doppler distribution allows us to single out the pure Doppler broadening from the other broadening mechanisms while the Lorentz and Voigt's distributions are the ones to be used in pure radiation damping and combined radiation and collision broadening conditions, respectively. For all these three lineshapes, the spectra can be written as a function of a dimensionless optical frequency defined as $x = \frac{\nu-\nu_0}{\Delta\nu}$. For the Doppler and Lorentz cases, this is a normalized difference to the centre of line frequency, where $\Delta\nu$ stands for the FWHM of the Doppler (or Lorentz) distribution at each given temperature. For the Voigt lineshape, the width parameter $\Delta\nu$ is the one for the underlying Doppler distribution and $a = \sqrt{\ln(2)}\frac{\Delta\nu^L}{\Delta\nu^D}$ is the Voigt characteristic width, the relative Lorentz over Doppler spectral width and implicitly dependent upon both temperature and vapour pressure.

2.2. Holstein–Biberman equation

The starting point for the majority of incoherent radiation trapping models is the *Holstein–Biberman equation* which is a Boltzmann-type integro-differential equation describing the spatial and temporal evolutions of the excited state number density $n(\boldsymbol{r}, t)$ as

$$\frac{\partial n(\boldsymbol{r}, t)}{\partial t} = -\Gamma n(\boldsymbol{r}, t) + \Gamma\phi_0\int_V f(\boldsymbol{r}, \boldsymbol{r}')n(\boldsymbol{r}', t)\,\mathrm{d}\boldsymbol{r}', \tag{1}$$

where the non-local character of trapping is evident in the last term of the right-hand side: a local excited number density increase owing to reabsorption of radiation emitted from all parts of the sample enclosure. ϕ_0 is the intrinsic (i.e. unaffected by trapping) emission quantum yield, and can be interpreted as the probability of photon emission by an excited state (the ratio of radiative over global relaxation rate constants: $\phi_0 = \frac{\Gamma_r}{\Gamma}$). $f(\boldsymbol{r}, \boldsymbol{r}')$ is the (conditional) transition probability of photon absorption at $\boldsymbol{r}$, given that there was an emission at $\boldsymbol{r}'$.

For the classical trapping problem [2], in which the time of flight of in-transit radiation between emission and reabsorption is negligible compared with the natural lifetime of the excited states, and for linear response conditions, two alternative ansatze can be used to obtain solutions for the previous equation: Holstein's exponential mode expansion and the so-called multiple scattering representation (MSR).

In the form presented in (1), the Holstein–Biberman equation neglects the time of flight of radiation and, therefore, the spatial and temporal dynamics are decoupled. Holstein proposed an eigenmode expansion

$$n(\boldsymbol{r}, t) = \sum_n n_n(\boldsymbol{r})\,\mathrm{e}^{-\beta_n t}, \tag{2}$$

as the general solution of (1). This solution, has, however several important shortcomings: (i) the eigenmodes (stationary spatial modes) $n_n(\boldsymbol{r})$ have a troublesome physical interpretation since all but the slowest decaying mode take negative values at some points and cannot thus be identified with physical distributions; (ii) individual relaxation constants β_n have no simple connection with physical parameters; (iii) the eigenmodes/values are not easily estimated;

and (iv) it is very difficult to generalize the mode expansion to account for additional effects (polarization, partial frequency redistribution between absorption and reemission, radiation propagation time, particle diffusion). However, an alternative mode expansion exists that overcomes most of these difficulties. It is known as the multiple scattering representation since it identifies each spatial mode with the spatial distribution of excited species after several scattering (reemission–reabsorption) orders. These multiple scattering modes are associated with several *generations* of excited species, paralleling the members of decaying radioactive families. The MSR was independently proposed for atomic [10] and molecular trapping [11] and, subsequently, proven to be equivalent to the original Holstein solution [12]. For general reviews see [2, 4].

Although the Holstein mode expansion is well known to the radiation transport specialist, its utility to a wider audience is hampered by the abovementioned shortcomings. In particular, it must be emphasized that the standard solution of (1) by a multiexponential expansion is in fact an eigenproblem which has an elementary solution algorithm (both mathematically and also from the point of view of physical intuition) only for the case of the slowest decaying mode. This is usually called the fundamental mode and its eigenvector corresponds to a relaxed spatial excitation distribution. However, the standard practice of substituting the whole of the dynamics for the fundamental mode alone is unsatisfactory since it does not fully describe the trapping phenomenon. Moreover, in common situations in steady-state applications, the fundamental mode introduces a systematic error in approximating the actual trapping influenced steady-state solution to (1). In order to go beyond the fundamental mode, a wealth of computational algorithms exist that were developed in recent decades (see [2]). However, to master at the same time both the physics, the computational algorithms, and the technical tricks of the trade is not an easy task. But perhaps more importantly, from a pedagogical point of view, it would be preferable for the student first to master the physics using a simple computational model. The MSR approach is in this respect very attractive since it is simpler and more amenable to discussion at an elementary level than the alternative Holstein multiexponential expansion. Its numerical implementation is straightforward and can be easily discussed at a level that stresses physical intuition without actually getting into the intricate details needed for the estimation of Holstein modes other than the fundamental. In its essence, it is just the estimation of mean reabsorption and escape probabilities. The theoretical formulation of the MSR stochastic model must weight properly these mean probabilities when quantifying the effect of trapping on observables. The way this is done is summarized in the following subsection.

2.3. Multiple scattering representation

In the MSR ansatz for linear incoherent trapping with a negligible time of flight for in-transit radiation, the spatial and temporal relaxation dynamics for excitation are given by

$$n(\boldsymbol{r}, t) = \sum_n a_n p_n(\boldsymbol{r}) g_n(t), \tag{3}$$

where n stands for the *generation number* of excited species (initial excitation creates the first generation, the trapping of this generation's emission creates a second generation and so on; one can envisage each generation as the result of $n-1$ previous scattering events of resonance radiation), a_n is the population efficiency for each generation, and $p_n(\boldsymbol{r})$ and $g_n(t)$ are the (normalized) spatial and temporal excited species distributions, respectively. The $p_n(\boldsymbol{r})$ s replace the eigenmodes of the Holstein ansatz with distinctive advantages since their physical interpretation is clear; they are the spatial distribution of excitation after $n-1$ scattering events. The temporal distributions are easily obtained for incoherent trapping; the temporal

evolution of each generation, $g_n(t)$, is an iterated convolution of the intrinsic response of each generation, $g(t) = \mathrm{e}^{-t}$. The temporal evolution is, therefore, $g_n(t) = \frac{t^{n-1}}{(n-1)!}\mathrm{e}^{-t}$ [4]. The trapping efficiency can be discussed either based on each generation's population efficiency a_n or, preferably, on each generation's reabsorption probability defined as $\alpha_n \equiv \frac{a_{n+1}}{a_n}$. One should elaborate a little further by factoring out trapping specific effects (opacity scales, geometry, spectral distribution) from the trivial influence of the reemission probability ϕ_0. This decoupling can be made by writing $\alpha_n \equiv \alpha_n^T \phi_0$ (superscript T signals quantities dependent only on trapping efficiencies) and $a_n = a_n^T \phi_0^{n-1}$ with $a_n^T = \prod_{n=1}^{n-1} \alpha_n^T$. Finally, one should be aware that only a fraction of the radiation emitted by each generation escapes (or, is reabsorbed); the generation-dependent mean escape probability can be defined as $q_n = \phi_0\left(1 - \alpha_n^T\right)$. With these aspects in mind, useful expressions can be derived for the relevant parameters of the ensemble.

2.3.1. Ensemble relaxation parameters. The trapping dynamics has a direct effect on the two single most important macroscopic parameters for the ensemble relaxation; the overall re-emission efficiency ϕ (mean photon re-emission probability out of sample enclosure, irrespective of scattering order) and mean excitation deactivation or photon emission lifetime τ (mean excitation survival time in macroscopic ensemble). These will be the most important quantities to be extracted from (3). Before showing explicitly how these quantities are obtained, let us consider the relaxation from an initially created population of excited species based on trapping alone. After a sufficiently high number of scattering events, initial excitation will relax to a distribution which, when normalized, does not change with time since each point deactivation is exactly balanced with local reabsorption due to emission from the whole ensemble. Thus, based on physical insight, in all of the following we can divide the contribution of all the generations in two groups: one summing up the spatial changing excited species and the other grouping all the generations with a nonchanging distribution (Holstein's fundamental mode with an analytical explicit sum; see discussion below). The generations will be grouped into up to $m = n_{nc}$ and m onwards, where the subscript is a remainder for *nonchanging*. The nonchanging distribution is stationary in the sense that it is time-independent but we will keep the nc subscript to emphasize the difference to the steady-state or *stationary* system response to a continuous perturbation and avoid common misinterpretations.

To obtain the ensemble dynamics, we will need to compute sums of the type $\sum q_n a_n$ or $\sum a_n p_n(\boldsymbol{r})$ and $\sum n q_n a_n$ and, in these, we will use the fact that $q_{n\geqslant m} = q_{nc}$, $p_{n\geqslant m}(\boldsymbol{r}) = p_{nc}(\boldsymbol{r})$ and $a_{n\geqslant m} = a_{nc}\alpha_{nc}^{n-m}$. The ensemble re-emission yield is

$$\begin{aligned}
\phi &= \int_0^{+\infty} \left[\sum_{n=1}^{+\infty} q_n a_n g_n(t)\right] \mathrm{d}t \\
&= \sum_{n=1}^{+\infty} q_n a_n \int_0^{+\infty} g_n(t)\,\mathrm{d}t \\
&= \sum_{n=1}^{+\infty} q_n a_n \\
&= \sum_{n=1}^{m-1} q_n a_n + \frac{q_{nc} a_{nc}}{\alpha_{nc}^m} \sum_{n=m}^{+\infty} \alpha_{nc}^n \\
&= \sum_{n=1}^{m-1} q_n a_n + \frac{q_{nc} a_{nc}}{\alpha_{nc}^m} \left[\sum_{n=1}^{+\infty} \alpha_{nc}^n - \sum_{n=1}^{m-1} \alpha_{nc}^n\right]
\end{aligned}$$

$$= \sum_{n=1}^{m-1} q_n a_n + \frac{q_{nc} a_{nc}}{\alpha_{nc}^m} \left[\frac{\alpha_{nc}}{1-\alpha_{nc}} - \alpha_{nc} \frac{1-\alpha_{nc}^{m-1}}{1-\alpha_{nc}} \right]$$

$$= \sum_{n=1}^{m-1} q_n a_n + \frac{q_{nc} a_{nc}}{1-\alpha_{nc}}, \tag{4}$$

since

$$\rho(t) = \sum_{n=1}^{+\infty} q_n a_n g_n(t), \tag{5}$$

is just the emission decay.

The mean lifetime is

$$\tau = \frac{\int_0^{+\infty} t\rho(t)\,\mathrm{d}t}{\int_0^{+\infty} \rho(t)\,\mathrm{d}t}. \tag{6}$$

The denominator is just the re-emission yield, while the numerator can be written as

$$\begin{aligned}
\int_0^{+\infty} t \left[\sum_{n=1}^{+\infty} q_n a_n g_n(t) \right] \mathrm{d}t &= \sum_{n=1}^{+\infty} q_n a_n \int_0^{+\infty} t g_n(t)\,\mathrm{d}t \\
&= \sum_{n=1}^{+\infty} n q_n a_n \\
&= \sum_{n=1}^{m-1} n q_n a_n + \frac{q_{nc} a_{nc}}{\alpha_{nc}^m} \left[\sum_{n=1}^{+\infty} n\alpha_{nc}^n - \sum_{n=1}^{m-1} n\alpha_{nc}^n \right] \\
&= \sum_{n=1}^{m-1} n q_n a_n + \frac{q_{nc} a_{nc}}{\alpha_{nc}^m} \\
&\quad \times \left[\frac{\alpha_{nc}}{(1-\alpha_{nc})^2} - \frac{\alpha_{nc}}{(1-\alpha_{nc})^2} \left((m-1)\alpha_{nc}^m - m\alpha_{nc}^{m-1} - 1 \right) \right] \\
&= \sum_{n=1}^{m-1} n q_n a_n + \frac{q_{nc} a_{nc}}{(1-\alpha_{nc})^2} [m(1-\alpha_{nc}) + \alpha_{nc}],
\end{aligned} \tag{7}$$

since each generation will decay on average in n units of the dimensionless time. Finally, the scaled lifetime is

$$\tau = \frac{\sum_{n=1}^{m-1} n q_n a_n + \frac{q_{nc} a_{nc}}{(1-\alpha_{nc})^2} [m(1-\alpha_{nc}) + \alpha_{nc}]}{\phi}. \tag{8}$$

2.3.2. Steady-state spectra and spatial distribution. The decay in (5) is strictly valid for a delta pulse excitation. However, under incoherent conditions, the decay for other initial excitation distributions is obtained from linear response theory as the convolution of the excitation profile with the delta response function (e.g. [13] and references therein). Let us obtain the system observables for a continuous excitation which constitutes a particularly important limiting case in many practical conditions. We have then *steady-state* or *stationary* conditions and use superscript SS to express it.

The overall emission intensity is just the previously computed macroscopic emission yield ϕ but now the most important quantity is the spectral distribution. To obtain it, the decay should be resolved both in the optical frequency and in the detection geometrical details. For

the most important case of complete frequency redistribution [2], both spectra, absorption and emission, are the same and therefore the decay is

$$\rho^{\Omega}(x,t) = \sum_{n=1}^{+\infty} \Phi(x) q_n^{\Omega}(x) a_n g_n(t). \tag{9}$$

The decay at each frequency depends upon the intrinsic spectrum $\Phi(x)$ and on the mean escape probability in the detection direction Ω,

$$q_n^{\Omega}(x) = \int_{\Omega}\int_{V} \mathrm{e}^{-\Phi(x)r}\, p_n(\boldsymbol{r})\, \mathrm{d}\boldsymbol{r}\, \mathrm{d}S, \tag{10}$$

where the Beer–Lambert escape (survival) probability is weighted in both spatial distribution inside volume V and over the surface S facing detection optics. r should be the optical distance between emission coordinate $\boldsymbol{r}$ and the surface point facing detection. In unidimensional geometry (see next section), photon escape to the left reduces to

$$q_n^{\Omega}(x) = \int \mathrm{e}^{-\Phi(x)r}\, p_n(r)\, \mathrm{d}r, \tag{11}$$

if one chooses to set the origin of the opacity scale on the left side of the cell.

Now the steady-state spectrum is obtained by time integrating this, giving

$$I^{SS,\Omega}(x) = \sum_{n=1}^{+\infty} \Phi(x) q_n^{\Omega}(x) a_n. \tag{12}$$

The distortion of emission spectrum owing to trapping is better appreciated if one scales the emission spectrum and it is thus better to have the normalized spectral distribution,

$$I^{SS,\Omega}(x) = \frac{\sum_{n=1}^{m-1} q_n^{\Omega}(x) a_n + \frac{q_{nc}^{\Omega}(x) a_{nc}}{1-\alpha_{nc}}}{\int_{-\infty}^{+\infty} \left[\sum_{n=1}^{m-1} q_n^{\Omega}(x) a_n + \frac{q_{nc}^{\Omega}(x) a_{nc}}{1-\alpha_{nc}}\right] \Phi(x)\, \mathrm{d}x} \Phi(x). \tag{13}$$

The numerator gives the trapping-dependent spectral distortion. At this point the paramount importance of the x-dependent escape probability in defining the contribution of each generation to the observed spectra must be stressed, this being due to the strong nonlinear character of (10).

It is also informative to know the steady-state spatial distribution. This can be obtained, again under the conditions of linear response theory, from the overall (reflecting all generation's contribution) time resolved normalized spatial distribution

$$\begin{aligned} n(\boldsymbol{r},t) &= \frac{\sum_{n=1}^{+\infty} a_n p_n(\boldsymbol{r}) g_n(t)}{\int \sum_{n=1}^{+\infty} a_n p_n(\boldsymbol{r}) g_n(t)\, \mathrm{d}\boldsymbol{r}} \\ &= \frac{\sum_{n=1}^{+\infty} a_n p_n(\boldsymbol{r}) g_n(t)}{\sum_{n=1}^{+\infty} a_n g_n(t)}. \end{aligned} \tag{14}$$

Time integrating both the numerator and the denominator of (14) gives

$$\begin{aligned} n^{SS}(\boldsymbol{r}) &= \frac{\sum_{n=1}^{+\infty} a_n p_n(\boldsymbol{r})}{\sum_{n=1}^{+\infty} a_n} \\ &= \frac{\sum_{n=1}^{m-1} a_n p_n(\boldsymbol{r}) + \frac{a_{nc}}{1-\alpha_{nc}} p_{nc}(\boldsymbol{r})}{\sum_{n=1}^{m-1} a_n + \frac{a_{nc}}{1-\alpha_{nc}}}, \end{aligned} \tag{15}$$

since the $g_n(t)$ are normalized.

In all of the above expressions, it is important to recognize that the trapping dynamics can be factored out into a generation varying part and another corresponding to generations that

have the same spatial distribution (the fundamental mode) and the nonchanging part can be expressed explicitly as an analytical sum. The dynamics for this nonchanging part corresponds only to an attenuation of overall excitation in going from one generation to the next by a fixed α_{nc} factor and, as a result, the contribution of this part corresponds to a monoexponential relaxation with a trapping-dependent effective decay constant.

3. Markov stochastic algorithm

We conducted a model study for atomic radiation trapping stressing physical insight and using only elementary computational concepts and resources. We have used a two-level single line atomic model with Doppler, Lorentz or Voigt spectral distributions. We have, furthermore, decided to use a unidimensional geometry, driven by the motivation to do a simple mimic of a cylindrical tube of a discharge fluorescence lamp and by the desire to keep computational detail and power adequate to the proposed audience of final undergraduate and beginning graduate students. In this 1D case, the opacity scale comes naturally as the opacity along the cylindrical axis. The simplest and most general case of complete frequency redistribution conditions is used [2], which means that the number of collisions during the lifetime of excited atoms is sufficiently high to render the reemitted photon's frequency completely uncorrelated with the frequency of the previously absorbed photon. Under these conditions, the absorption and emission lineshapes coincide and the jump length distribution of the excitation random trajectory is independent of previous jumps. This makes the formalism of Markov processes [14] especially adequate. Its rationale for the MSR implementation can be cast in the following way. The 1D cell is divided into several bins, each corresponding to a *pure state* of the system and characterized by a mean probability that the excitation resides in that state. The system dynamics corresponds to the evolution of the probability of excitation being inside each state. The stochastic process is completely specified by (i) a column vector with the (normalized) spatial probability distribution of the first generation species, $\boldsymbol{p}_1 = \left[p_1^i\right]$ and (ii) a transition matrix $\boldsymbol{P} = [p^{ij}]$, whose entries are the *one-step* transition probabilities between states i and j. For a complete frequency redistribution, there is an absence of memory effects (homogeneous chain) meaning that the transition probability between individual states depends only upon their relative opacity distance (it is independent of the generation number and thus computed only once).

The binning of the spatial excitation distributions corresponds to the substitution of a continuous distribution for its discretized version, effectively transforming a continuous process into a discrete one realized in a lattice. It is, therefore, the Markov equivalent of a random walk defined over a regular spaced lattice [15] and the binning corresponds to the single most important approximation underlying the use of the Markov model. The bin width (or the number of cells) is the critical parameter for the algorithm. We have conducted several tests and found it advisable to have a maximum bin size of 0.05 in an opacity scale. Otherwise, numerical artifacts associated with substituting the actual excitation migration for the jump between the mean coordinates of each bin of sample cell could exist. These were found to be more important for higher overall opacities.

We have mentioned in the last section that the stochastic formulation of the MSR model aims at estimating mean reabsorption and escape probabilities. These are straightforwardly estimated from each generation's spatial distribution. The Markov algorithm proceeds then in four consecutive steps: (i) specify the first generation's spatial distribution and the transition matrix (the system relaxation response due to radiation trapping), (ii) compute each generation's spatial distribution from the previous generation's counterpart, (iii) estimate

each generation's mean reabsorption and escape probabilities and, finally, (iv) compose the overall ensemble data from each generation's relative contribution.

3.1. Spatial distribution of the excitation

The spatial distribution functions for all the generations are calculated from the previous generation by

$$\boldsymbol{p}_{n+1} = \boldsymbol{P}\boldsymbol{p}_n. \tag{16}$$

The sample cell is divided into h-length bins and the transition matrix elements are, therefore, given for a 1D geometry by [16]

$$p^{ij} \simeq \frac{1}{2}h\int_{-\infty}^{+\infty} \Phi^2(x)\,\mathrm{e}^{-\Phi(x)|r_i - r_j|}\,\mathrm{d}x, \tag{17}$$

corresponding to the Beer–Lambert law weighted according to the emission lineshape for an individual reemission–reabsorption (scattering) event. The integration takes into account all the possible emission frequencies, $1/2$ is the left or right emission direction probability for a 1D geometry and it was assumed that the bin width is sufficiently small in order to attain a satisfactory precision.

The complete specification of the Markov process is achieved once one specifies the initial spatial distribution $\boldsymbol{p}_1$. Since we wanted to discuss the excitation relaxation dynamics for conditions mimicking electron impact as well as photoexcitation, we considered two possibilities for the first generation. In the first case, we used homogeneous initial excitation (trivial; electron impact), while for the second case we considered photoexcitation with the reabsorption undistorted line (this last case corresponds to a common experimental practice; see for instance [17]). For photoexcitation from the *left* side of the 1D cell,

$$p_1^i \simeq h\int_{-\infty}^{+\infty} \Phi^2(x)\,\mathrm{e}^{-\Phi(x)r_i}\,\mathrm{d}x, \tag{18}$$

which afterwards must be properly normalized.

The numerical integrations are necessary to estimate both transition probabilities and the first generation's distribution for the case of photoexcitation, equations (17) and (18), must map the infinite domain of integration into a finite representation in the computer. One simple purely numerical way to achieve this is demonstrated in [18]. This is an important point owing to the need of accounting for the so-called wings of the spectral distribution, those with the most important contribution to excitation spreading due to reabsorption of resonance radiation on higher opacity scales.

Equation (16) is equivalent to linear response theory and, therefore, the evolution of the spatial excitation is given as a convolution integral between the *excitation profile* $\boldsymbol{p}_n$ with the *delta response function* given by (17). This renders the Markov approach especially efficient since this convolution can be easily made using FFT algorithms [19] paying attention to zero pad to double size the column vector containing the excitation distribution in order to avoid wrap-around effects due to the cyclic convolution [18]. The speed-up factors could rise up to several orders of magnitude (roughly 50 to 400 times for a number of Markov states of 2 000 to 200 000) making the FFT convolution the recommended implementation of the Markov algorithm. The instructor has the freedom to tailor the computational physics project as needed by using either a direct matrix multiply or, alternatively, a FFT-based convolution approach to (16).

3.2. Reabsorption and escape probabilities

The mean reabsorption and escape probabilities for each generation are estimated from their spatial excitation distribution. The reabsorption probabilities are estimated with the following procedure. One starts with a normalized spatial distribution for the first generation. Then, each time (16) is used, the fraction of the excitation remaining inside the sample cell gives the nth generation mean reabsorption probability: the sum over all the states i—$\alpha_n^T = \sum_i p_{n+1}^i$—immediately after using (16). The excitation column vector is then (re)normalized and the process repeated. From the values of this parameter for each generation, the trapping population efficiency is $a_n^T = \prod_{n=1}^{n-1} \alpha_n^T$. This procedure is the equivalent of an important sampling method in a Monte Carlo simulation, in which it is assumed a unit intrinsic reemission yield in (17). The Markov algorithm directly estimates a_n^T, each generation's population efficiency due to trapping (and geometry) alone, and the actual population efficiencies were then given by $a_n = a_n^T \phi_0^{n-1}$. As for the escape probabilities, we suggest the following implementation of (11). The monochromatic left escape probability is obtained from

$$q_n^{\Omega}(x) = \boldsymbol{Q}(x)\boldsymbol{p}_n, \tag{19}$$

where $\boldsymbol{p}_n$ is the spatial distribution and $\boldsymbol{Q}(x)$ is the escape matrix, whose entries are finally,

$$q^{i\Omega}(x) \simeq \tfrac{1}{2}\, \mathrm{e}^{-\Phi(x) r_i}, \tag{20}$$

which comes from the Beer–Lambert law.

3.3. Fundamental mode

The estimation of parameters for each generation (spatial distribution and mean reabsorption and escape probabilities) is done as described in the two previous subsections. Nevertheless, the practical question of defining a *figure-of-merit* or *objective* function to estimate the fundamental mode remains. This is especially important for high opacity cases since we have found that for high overall opacities, a small error in the fundamental mode can be greatly amplified in the ensemble relaxation parameters. The single criterion we advise to use as a test for convergence to the fundamental mode with the generation number is the mean reabsorption probability. That this is the most useful criterion can easily be justified from both the physical meaning of the fundamental mode and the nature of the Markov algorithm. The Markov stochastic formulation considers directly the evolution of *mean* excitation probabilities. The evolution of the mean spatial distribution is considered whenever applying (16). By repeating this equation one mimics the relaxation of excitation from the initial distribution into a nonchanging spatial distribution, precisely the sought for fundamental mode distribution. The relaxed nonchanging spatial distribution is a vector quantity but the corresponding mean reabsorption probability is a single scalar number that we can test for the attainment of the limiting spatial distribution. We have made several tests and ended up using a conservative fractional tolerance of 10^{-6} for the mean reabsorption probability of the generation corresponding to the fundamental mode distribution. So the Markov chain simulation proceeded as follows: (i) we considered the initial excitation spatial distribution; (ii) repeatedly applied (16) to estimate for each generation the mean probabilities and renormalize; (iii) for each generation we tested the mean reabsorption probability for convergence and decided either to continue applying (16) or to end up due to convergence to the fundamental mode. After having reached the *nonchanging* mode, we took into account its analytical contribution to the ensemble obervables in equations (4), (8), (13) and (15).

3.4. Excitation spatial distribution functions

The mean reabsorption and escape probabilities for each generation are scalar quantities and, thus, pose no special demands on computer memory resources. However, this is not the case for the spatial distribution functions. We have mentioned before that the binning of these distributions is the single most important approximation in the Markov algorithm and stressed the need to use a binning as small as 0.05 in opacity. So each generation's spatial distribution is a vector valued quantity and possibly a very big one. The algorithm proceeds by following each generation's spatial distribution until convergence to the nonchanging mode. This mode could correspond to generation numbers as high as some hundreds (see the discussion of results), thus eventually posing some constrains on memory. The recommended solution to circumvent this difficulty is not to record all the spatial distributions but only the last two, the previous and the current one. In addition to these two, only one more vector is needed: the one used to record the steady-state spatial distribution. During the intermediate generation computations, one uses this vector to keep track of the accumulated contribution of generations up to the present generation number: the first term in the numerator of (15). After reaching the fundamental mode, this equation is finally updated with its relative contribution (the last term in the numerator) and the distribution properly normalized (the denominator). For the remaining quantities, the simplest procedure is to keep in memory the probability values for all the generations up to the fundamental mode.

4. Results and discussion

4.1. Ensemble relaxation

Figure 1 shows the overall relaxation parameters for an initial homogeneous excitation and an intrinsic quantum yield of $\phi_0 = 0.9$ as a function of opacity for Doppler, Voigt and Lorentz lineshapes. The higher the opacity the more important the trapping is, with the following implications: (i) an increase of the mean relaxation time (equivalent to a mean number of scattering events before escape) and (ii) a decrease of the ensemble reemission yield (the fraction of original excitation that eventually comes out; an increased importance of trapping translates into additional possibilities of nonradiative relaxation). The Voigt continuous transition from Doppler into Lorentz is evident as well as the relative importance of core and wings of the distributions. The higher the Lorentz character of the spectra the higher the weight of the wings and the higher the escape probabilities (lower mean lifetime and higher macroscopic emission yield).

The model study used a two-level single line atomic model with Doppler, Lorentz or Voigt spectral distributions and particular attention is paid to the influence of the lineshape on the trapping efficiency. The Voigt case illustrates the fact that a continuous variation of the characteristic width parameter will map the Doppler into the Lorentz distributions by changing the relative importance of the Lorentz-like wings over the Doppler-like core of the distribution (figure 2). Accordingly, the ability to compute the Voigt line to machine precision is mandatory and we give some implementation details in the appendix.

Figures 3 and 4 show the mean scaled lifetime and reemission yield for a homogeneous initial excitation for the Doppler and Lorentz limiting spectral distributions, respectively, for several values of the intrinsic quantum yield. Three main conclusions can be drawn from these results. First of all, the two most important parameters controlling trapping efficiency are the spectral distribution and the value of ϕ_0. The higher the overall opacity the more difficult is the escape of radiation for Doppler-like distributions and the more important the escape from the Lorentz-like wings of the distribution. Second, trapping for Doppler-like

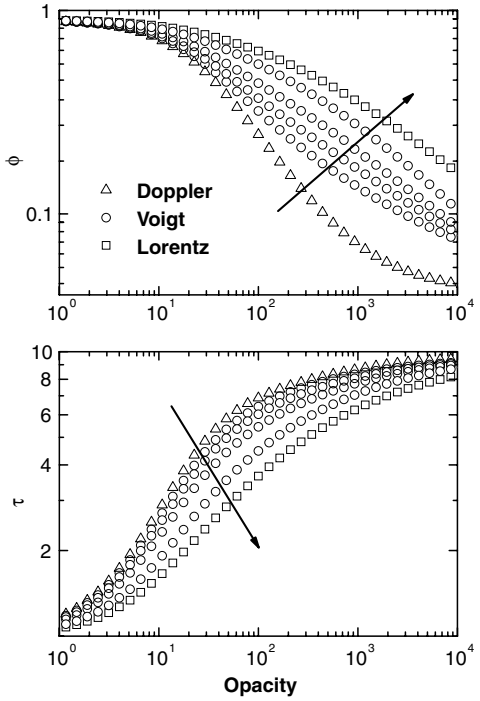

Figure 1. Reemission yield ϕ and mean scaled lifetime τ, with $\phi_0 = 0.90$ for Doppler, Voigt $a = 0.05, 0.1, 0.2$ and 0.5 and Lorentz lineshapes (direction shown by arrow).

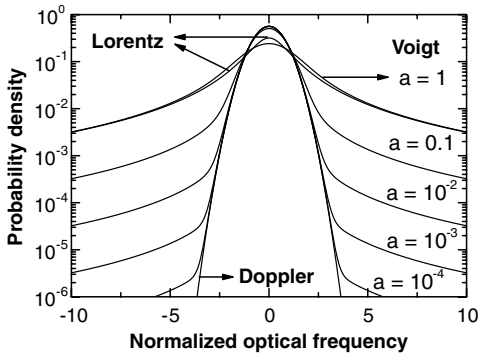

Figure 2. Doppler, Lorentz and Voigt lineshapes.

distributions is much more efficient since, especially in high opacity cases, the escape of excitation at optical frequencies far from the line centre frequency is reduced due to the extremely small probability of reemission at these frequencies (for unit reemission yield, the lifetime for the higher opacity is about 200 for Doppler and only about 15 for Lorentz). Finally, under conditions rendering trapping efficient, the ϕ_0 value is of paramount importance; for unit intrinsic reemission probability all the excitation will eventually come out (thus giving a simple check for consistency of computation) but, as soon as ϕ_0 is smaller than one, each new scattering event gives the excitation another chance of thermal degradation (in (4) each generation's contribution is intrinsically dependent upon ϕ_0^{n-1}). Note in these figures that

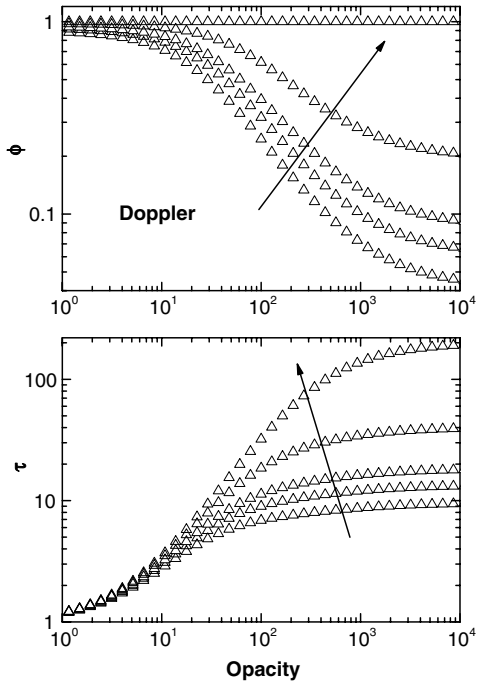

Figure 3. Reemission yield ϕ and mean scaled lifetime τ for the Doppler lineshape, with ϕ_0 values of 0.90, 0.93, 0.95, 0.98 and 1.0 (direction shown by arrow).

there is a strong dependence of the relaxation parameters on the ϕ_0 value, especially for the more trapping influenced Doppler case.

All these conclusions are important in the discussion of atomic vapour ensembles for lighting applications, either electric discharge lamps or plasma display panel (PDP) devices. Better performance is achieved with higher macroscopic reemission yields. On top of that, the increase of the overall opacity is in principle desirable since this is related to the increase of the number of excited species. In a crude first-order approximation, one can assume the overall lamp efficiency to be directly proportional to the product of ϕ times the overall opacity (directly proportional to initial excitation density):

$$\Psi \propto \phi \times r. \tag{21}$$

The actual behaviour of a lamp or a PDP can be quite involved since an increase in opacity means an increase of partial vapour pressure (the external dimensions of the device are fixed) and this induces several changes whose influence on the overall performance can be contradictory. The higher opacity means higher light throughput but only *as long as* the increase in the trapping efficiency does not substantially increase thermal degradation. The higher opacity could increase collisional deactivation to the point that its overall influence to light throughput is undesirable. To have a simple idea of the effect, and due to the paramount importance of the reemission quantum yield ϕ_0, a series of results were made for both limiting Doppler and Lorentz distributions with the radiative quantum yield given by $\phi_0 = \frac{\Gamma_r}{\Gamma_r+\Gamma_q}$, where the quenching rate constant was assumed in a first order approximation to be linear with the cell opacity ($\Gamma_q \equiv kr$, with the numerical values $\Gamma_r = 10^7\ \mathrm{s}^{-1}$ and $k = 2.5 \times 10^4\ \mathrm{s}^{-1}$). This corresponds to the well known Stern–Volmer equation for dynamical quenching by binary collisions for unitary intrinsic radiative yield in the absence of collisions. The results

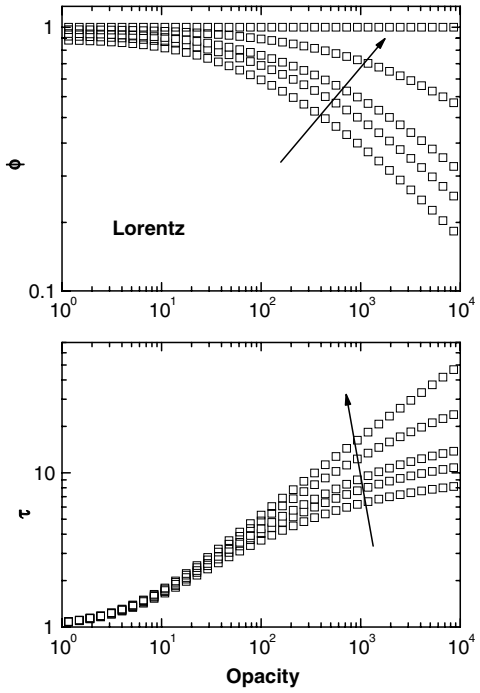

Figure 4. Reemission yield ϕ and mean scaled lifetime τ for the Lorentz lineshape, with ϕ_0 values of 0.90, 0.93, 0.95, 0.98 and 1.0 (direction shown by arrow).

are shown in figure 5 which is judged to be more representative of the actual lamp behaviour than the results in figures 3 and 4. Figure 5 shows that, ultimately, a delicate balance will dictate the best operation conditions which manifest themselves in the peaks of the Ψ values. Of course, the results are very approximate since the assumed functional dependence of ϕ_0 is only approximate. Nevertheless, figure 5 allows the discussion of the qualitative behaviour emphasizing physical insight without the additional burden of fine grained details. It shows how critical the spectral distribution shape and the quantum reemission yield are. For ϕ_0 values sufficiently close to one, an increase in opacity corresponds to an increase in lighting efficiency due to the increased initial excitation number density. However, as soon as the ϕ_0 value starts to be significantly smaller than one, the trapping leads to a much higher thermal degradation (compare the difference between the quantum and the ensemble yield or the reduced overall relaxation lifetime in the upper part of figure 5) which, ultimately decreases the lighting efficiency. From some point onwards this will be more important than the increase in initial excitation due to a higher vapour pressure, which originates optimal operation conditions, giving the best possible lighting efficiency. Figure 5 also shows that the Doppler distribution is associated with smaller throughput in lighting applications when compared with the Lorentz case due to the step reduction of the ensemble reemission yield with the increase of the overall opacity. This could of course be related to the use of an inert gas filling to render collisions more important (increasing the Lorentz character of the spectral distribution and reducing trapping efficiency) in fluorescence lamps.

The results of figure 5 allow a semi-quantitative discussion of a multitude of physical effects motivated by lighting applications without introducing any qualitative difference in the basic Markov algorithm; the only modification is the underlying approximation in the form

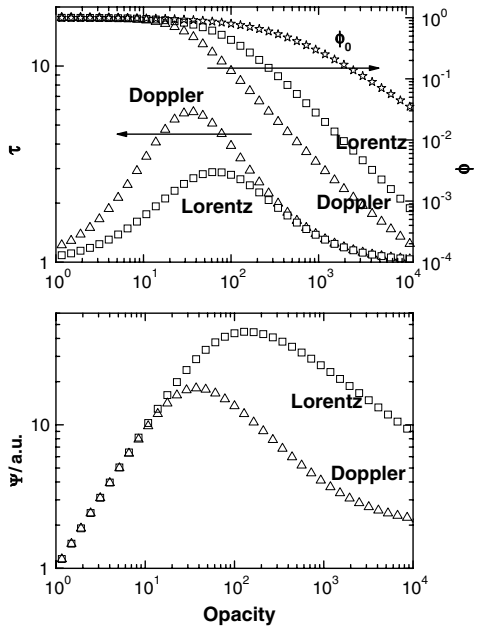

Figure 5. Ensemble relaxation parameters as a function of overall opacity for Doppler and Lorentz lineshapes. The upper part shows the reemission yield ϕ and mean scaled lifetime τ while the lower part shows the predicted relative efficiency for lighting applications estimated from (21). ϕ_0 is implicitly dependent upon opacity (upper part and text).

of (21). This equation permits some discussion of the role of collisional deactivation and its relation to the trapping efficiency without added computational complexity. The suggested model should, thus, be useful if the instructor wants to be more detailed in the discussion of additional physical effects. Of course, she may choose not to implement (21) without losing the essential.

Finally, figure 6 shows the predicted ensemble relaxation parameters for both homogeneous and photoexcitation as a function of overall opacity. Up to opacities of the order of 10, no significant difference exists (photoexcitation is able to penetrate well deep into sample cell). But, for higher opacities, the importance of trapping continues to increase indefinitely for the homogeneus excitation while it levels off for photoexcitation, a point to be revisited in section 4.3 when discussing spatial distribution functions.

4.2. Steady-state spectra

Figure 7 shows the estimated normalized spectral distribution in steady-state conditions for Doppler, Lorentz and Voigt lineshapes for both primary homogeneous and photoexcitation. The motivation for the homogeneous case is the excitation along the axis of a fluorescence lamp for lighting applications. It shows the well known self-reversal of spectral lines due to the higher attenuation of core optical frequencies. For photoexcitation, there is a balance between reduced penetration of external excitation and higher attenuation at core frequencies which dictates a flattening of the spectra near the line centre (of course, for left wall photoexcitation and right wall detection there is a self-reversal higher than the one for homogeneous excitation; not shown). In both cases, there is a considerable broadening of the detected spectra and the

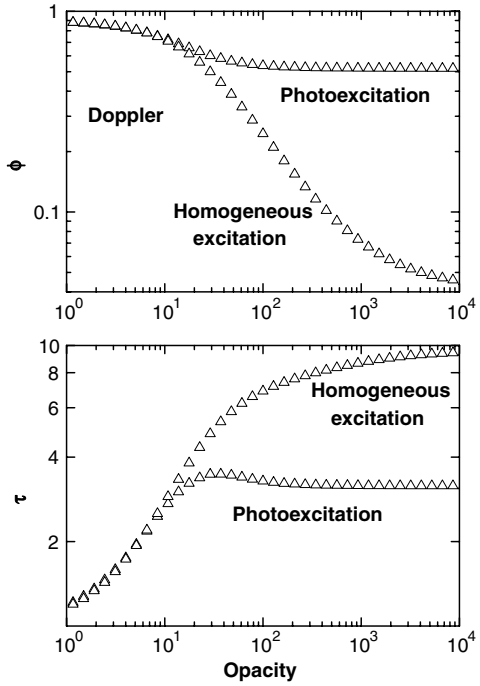

Figure 6. Reemission yield ϕ and mean scaled lifetime τ for the Doppler lineshape with $\phi_0 = 0.90$, for homogeneous and external photoexcitation (with the reabsorption undistorted line).

Voigt distribution has an intermediate character between core Doppler-like and wings Lorentz-like.

4.3. Spatial distribution

Figure 8 shows the steady-state spatial distributions for both limiting cases of Doppler and Lorentz distributions. This figure shows that the fundamental mode spatial distribution (limiting case for a relaxed, non-changing spatial distribution and thus independent of the original excitation) could only give a reasonable approximation of the steady-state distribution for the homogeneous excitation case; for photoexcitation it is more convenient to choose the spatial distribution of the first generation species as a first approximation to the overall distribution. This illustrates the well known procedure of, whenever approximating the actual trapping-dependent behaviour by the monoexponenial fundamental mode (easier to obtain by a variational procedure or given by Holstein's asymptotic approximations), design the experimental setup to mimic as much as possible the fundamental mode spatial distribution (symmetrical and well spread into the bulk of sample cell) with the external excitation. This can be accomplished with photoexcitation of high opacity samples using strongly detuned external radiation.

4.4. Fundamental mode

Figure 8 shows some of the problems of quantifying trapping simply by using the fundamental mode, a point further illustrated in table 1. Several conclusions can be drawn from its data: (i) Doppler distributions render trapping much more efficient and thus its fundamental mode

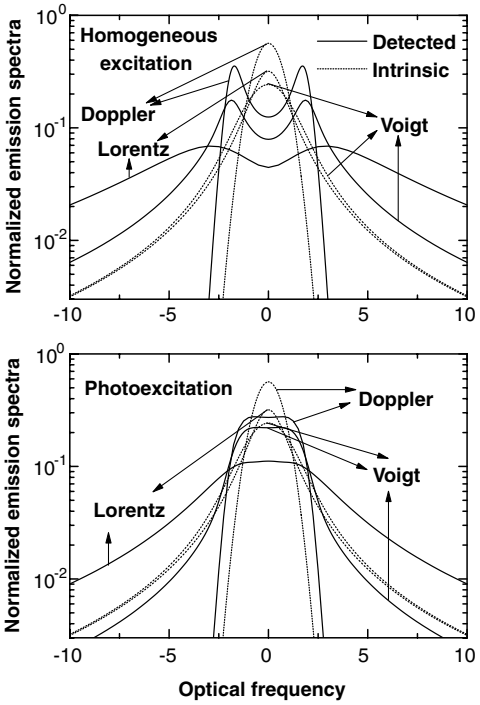

Figure 7. Normalized steady-state spectra for Doppler, Lorentz and $a = 0.1$ Voigt lineshapes for an overall opacity of 100 and $\phi_0 = 0.90$. The photoexcitation case corresponds to both excitation and detection from the left cell wall using the reabsorption undistorted line for photoexcitation.

Table 1. Fundamental mode contribution to the reemission yield ϕ and mean scaled lifetime τ. The approximate generation number corresponding to the fundamental mode (m), for a 10^{-6} fractional tolerance to consider a non-changing spatial distribution is also shown (see text). In all cases, $\phi_0 = 1$.

	Homogeneous						Photoexcitation					
	Doppler			Lorentz			Doppler			Lorentz		
Opacity	m	ϕ	τ	m	ϕ	τ	m	ϕ	τ	m	ϕ	τ
10	10	6%	20%	7	1%	3%	10	3%	14%	7	1%	3%
100	70	10%	40%	30	0.5%	3%	100	2%	20%	35	0.1%	1%
1000	200	25%	60%	80	1%	6%	550	0.2%	6%	100	0.1%	1%

contribution is always much higher than that for the Lorentz case; (ii) the spatial spreading for Doppler is smaller, giving rise to a higher generation number for the fundamental mode; (iii) the use of the fundamental mode alone for Lorentz distributions (and therefore, albeit with a lesser degree, for Voigt) is never justified; and (iv) to approximate the actual behaviour for photoexcitation to the fundamental mode is never justifiable.

Two additional points related to the common practice of using only the fundamental mode to take into account trapping distortions should be emphasized. First, the fundamental mode is the slowest decaying possible and is located well (and symmetrical) into the sample cell. To substitute the whole of the ensemble dynamics for the fundamental mode alone will always overestimate the lifetime, and underestimate the reemission yield (spatial distribution

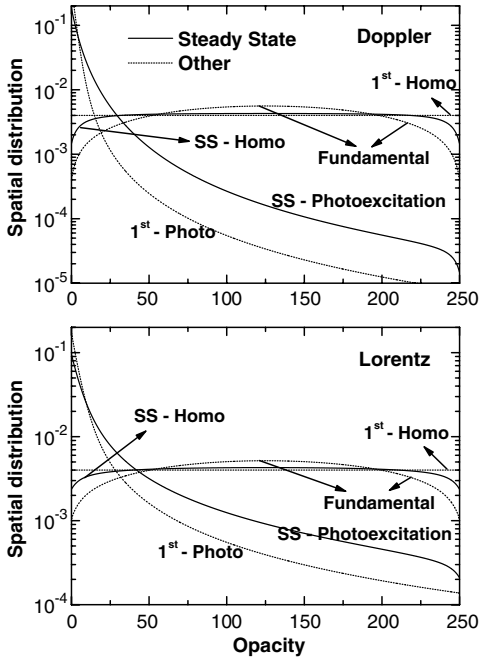

Figure 8. Normalized spatial distributions of excitation in steady-state (SS) conditions for Doppler and Lorentz lineshapes for an overall opacity of 250 and $\phi_0 = 0.90$. The primary excitation (homogeneous or photoexcitation) as well as the fundamental mode distributions are also shown. The photoexcitation case corresponds to both excitation and detection from the left cell wall using the reabsorption undistorted line for photoexcitation.

giving the highest possible trapping efficiency) thus introducing a systematic error. Secondly, the use of the fundamental mode alone is too often misunderstood with the use of the asymptotic approximations proposed by Holstein [20], only valid in the high opacity limit and for ideal geometries [2]. The MSR has a clear cut advantage relative to the Holstein approximation in this respect since it allows an easy estimation of the fundamental mode by elementary computational algorithms as that corresponding to a nonchanging spatial distribution, irrespective of opacity and geometry.

The spatial distribution functions presented in this section draw some further insights into the previous results of figure 6. The levelling of the lifetime and reemission yield at higher opacities for the photoabsorption case corresponds to absorption of external excitation complete within a layer smaller than the overall opacity making the ensemble relaxation effectively insensitive to the overall opacity. This approaches well the conditions of semi-infinite geometry, under the time scale of ensemble complete relaxation.

5. Conclusions

This contribution presented a unidimensional computational model study for complete frequency redistribution linear incoherent atomic radiation trapping that could constitute a general scaffold to base a computational physics project for final undergraduate or beginning graduate students. It is versatile enough for the instructor to adapt to specific needs while allowing some freedom to the student to explore additional effects both at a level of strict

computational physics algorithms, and at a level giving more emphasis to physical insight. Two examples of these additional further exploration issues could be the fast Fourier transform implementation of convolutions for the first case, or the detailed analysis of the collisional deactivation and trapping effects for steady-state lighting applications, for the second.

The model study tries to introduce the practical problem of incoherent resonance radiation reabsorption at a level adequate to the nonspecialist but nevertheless retaining the essential of all the physical effects. It goes beyond the standard but generally unjustifiable approximation of discussing trapping based only on an effective exponential mode for the ensemble relaxation. It illustrates the advantages of the multiple scattering representation (MSR) over the more well-known Holstein expansion, based on physical insight and computation feasibility at an elementary level. Holstein's ansatz has significant shortcomings when compared to the equivalent alternative of MSR: (i) Holstein spatial modes are unphysical except for the fundamental; (ii) their estimation is computationally much more troublesome than the simple algorithms used in this work; (iii) the wide spread use of original Holstein expressions for the fundamental mode are only valid in the asymptotic limit of high opacities while MSR allows an easy estimation of the fundamental at any opacity value; and (iv) the higher Holstein modes are difficult to obtain while for Lorentz-like spectral distributions we found that their contribution must be always taken into account (the fundamental mode contribution to ensemble relaxation being always small; higher Holstein modes correspond in the MSR language to small numbered generations and are easy to obtain with the stochastic formulation presented).

The dependence of the ensemble reemission yield and lifetime, relative efficiency for lighting applications, steady-state spectral and spatial distributions on reemission yield, opacity and homogeneous or external photoexcitation are discussed at length for the Doppler, Voigt and Lorentz lineshapes. We quantify the contribution of the nonchanging fundamental mode and found it uniquely troublesome using this mode for Voigt and Lorentz-like spectra. The results are comprehensive and try to provide as broad as possible range of possible exploration directions of the basic model study. They should appeal to a broad audience and provide insight into a wide range of more realistic situations in an atomic as well as in an astrophysical context, while maintaining the computational concepts and resources at a relatively modest level.

Acknowledgments

This work was supported by Fundação para a Ciência e Tecnologia (FCT Portugal) and Universidade do Minho (Portugal) within project REEQ/433/EEI/2005. It also used computational facilities bought under project POCTI/CTM/41574/2001, funded by FCT and the European Community Fund FEDER. AR Alves-Pereira acknowledges FCT funding under the reference SFRH/BD/4727/2001. E Nunes-Pereira acknowledges the critical reading of the manuscript by M Belsley (Centro de Física, Universidade do Minho).

Appendix. Numerical Voigt distribution

The numerical evaluation of the Voigt spectral distribution can be troublesome, as one can easily judge from the large number of approximations that have been published in recent decades balancing precision and computational speed (see [2] and references therein). This is especially true for the wings of the distribution in case of trapping since the photons can most easily escape via the wings, especially in high opacity vapours. However, given the current desktop computing capabilities, the numerical (careful) direct integration of the defining

equation is perfectly adequate and the use of approximations to reduce computation time is not justifiable any more. The difficulty in the direct numerical integration came from the behaviour of the integrand function: it differs from zero over two width scales, a broad scale centred at zero (corresponding to the exponential term in the numerator of the integrand) and a much narrower one centred in a frequency corresponding to the Voigt frequency (associated with the difference term in the denominator). The integration domain should therefore be broken into smaller domains and an automatic adaptative integration algorithm should be used in each subdomain always starting at the integrand function maximum and with an initial stepsize adapted to the local scale of variation of the integrand [18]. We have used the 400 central frequencies for the central broad feature and a 0.4 frequency width for the floating narrow peak. Integrations further away from the central core were analytically mapped from an infinite to a finite integration range. In order to decrease the time for repetitive Voigt function evaluations, the Voigt distribution was previously computed in a given table of frequency values and, whenever necessary, a cubic spline interpolation was used [18]. We used a linear scale in the core (frequency range up to 100 with a 5×10^{-2} spacing) and a log scale in the wings (frequency range from 100 to 10^8 with a $1 \times 10^{-3}\log_{10}$ spacing). Natural cubic spline was not necessary since the derivatives of the Voigt distribution in the end points are analytical.

References

[1] Mihalas D 1978 *Stellar Atmospheres* 2nd edn (San Francisco: Freeman)
[2] Molisch A F and Oehry B P 1998 *Radiation Trapping in Atomic Vapours* (Oxford: Oxford University Press)
[3] Thomas G E and Stamnes K 1999 *Radiative Transfer in the Atmosphere and Ocean* (Cambridge: Cambridge University Press)
[4] Berberan-Santos M N, Pereira E and Martinho J M G 1999 Dynamics of radiative transport *Resonance Energy Transfer* ed D L Andrews and A A Demidov (Chichester: Wiley) p 108
[5] Modest M F 2003 *Radiative Heat Transfer* 2nd edn (New York: Academic)
[6] Bardou F, Bouchaud J P, Aspect A and Cohen-Tannoudji C 2002 *Lévy Statistics and Laser Cooling* (Cambridge: Cambridge University Press)
[7] Lister G G, Lawler J E, Lapatovich W P and Godyak V A 2004 *Rev. Mod. Phys.* **76** 541
Proud J M and Luessen L H (eds) 1986 *Radiative Processes in Discharge Plasmas (NATO ASI Series, Series B Physics)* (New York: Plenum)
Waymouth J F 1971 *Electric Discharge Lamps* (Cambridge, MA: MIT Press)
[8] Rajaraman K and Kushner M J 2004 *J. Phys. D: Appl. Phys.* **37** 1780
[9] Rauf S and Kushner M J 1999 *J. Appl. Phys.* **85** 3460
Rauf S and Kushner M J 1999 *J. Appl. Phys.* **85** 3470
van der Straaten T and Kushner M J 2000 *J. Appl. Phys.* **87** 2700
[10] Falecki W, Hartmann W and Wiorkowski P 1989 *Z. Phys.* D **14** 111
[11] Martinho J M G, Maçanita A L and Berberan-Santos M N 1989 *J. Chem. Phys.* **90** 53
[12] Lai R, Liu S L and Ma X X 1993 *Z. Phys.* D **27** 223
Lai R, Liu S L and Ma X X 1993 *Opt. Commun.* **99** 316
[13] Berberan-Santos M N and Martinho J M G 1992 *Chem. Phys.* **164** 259
[14] van Kampen N G 1992 *Stochastic Processes in Physics and Chemistry* (Amsterdam: North-Holland)
Gardiner C W 1985 *Stochastic Processes in Physics and Chemistry* 2nd edn (Berlin: Springer)
[15] Hughes B D 1995 *Random Walks and Random Environments* vol 1 *(Random Walks)* (Oxford: Oxford University Press)
[16] Pereira E, Martinho J M G and Berberan-Santos M N 2004 *Phys. Rev. Lett.* **93** 120201
[17] van de Weijer P and Cremers R M M 1985 *J. Appl. Phys.* **57** 672
[18] Press W H, Teukolsky S A, Vetterling W T and Flannery B P 1992 *Numerical Recipes in Fortran, The Art of Scientific Computing* 2nd edn (Cambridge: Cambridge University Press)
Press W H, Teukolsky S A, Vetterling W T and Flannery B P 1996 *Numerical Recipes in Fortran 90, The Art of Parallel Scientific Computing* (Cambridge: Cambridge University Press)
[19] Frigo M and Johnson S G 2005 The design and implementation of FFTW3 *Proc. IEEE* **93** 216
[20] Holstein T 1947 *Phys. Rev.* **72** 1212